ChemComm

In Situ Identification of Cation-Exchange-Induced Reversible Transformations of 3D and 2D Perovskites

Journal:	*ChemComm*
Manuscript ID	CC-COM-04-2018-002801.R1
Article Type:	Communication

Chemical Communications

COMMUNICATION

In Situ Identification of Cation-Exchange-Induced Reversible Transformations of 3D and 2D Perovskites

Received 00th January 20xx,
Accepted 00th January 20xx

DOI: 10.1039/x0xx00000x

www.rsc.org/

Weixin Huang,[a,b] Subha Sadhu,[a] Pitambar Sapkota,[a,c] and Sylwia Ptasinska*[a,c]

The optical and structural properties of hybrid perovskites can be tuned by the post-synthetic introduction of new cations. To advance the development of this approach, knowledge of the reaction mechanism is essential, but has not yet been elucidated. Here, the effect of n-octylamine on three-dimensional (3D) methylammonium lead bromide ($MAPbBr_3$) was investigated by *in situ* X-ray photoelectron spectroscopy. Spectroscopic analysis indicated equimolar substitutions between octylammonium (OcA^+) and methylammonium cations (MA^+) that cause the formation of two-dimensional (2D) octylammonium lead bromide ($(OcA)_2PbBr_4$). The introduction of methylamine reversed these changes, and the cation exchange between MA^+ and OcA^+ caused the reverse conversion to $MAPbBr_3$.

Hybrid organic-inorganic perovskites (e.g., $MAPbX_3$, $MA^+ = CH_3NH_3^+$, X = Cl, Br or I) have achieved tremendous success in optoelectronic and photonic devices because of their outstanding optical and electrical properties.[1–3] Despite the rapid improvements in the solar cell efficiency of three-dimensional (3D) $MAPbX_3$, their chemical stability remains among the challenges that has hampered their widespread applications in actual devices.[4] It has been reported that $MAPbX_3$ films decompose rapidly after exposure to moisture, oxygen, heat, light, and low-energy electrons.[5–9] Substantial efforts have been made to address the stability problems of $MAPbX_3$ perovskite solar cells.[10,11] Because of their excellent environmental stability, two-dimensional (2D) organic-inorganic perovskites have emerged as a promising light absorber in photovoltaics.[12] 2D perovskites have a general formula of $(RNH_3)_2(MA)_{n-1}Pb_nX_{3n+1}$, in which the long-chain cations (RNH_3) serve as ligands to partition the inorganic lattice. In addition to their improved material stability, the bandgap of 2D perovskites can be tuned due to the quantum confinement effect.[13–16] By controlling the layer number "n", a fine tunability in exciton absorption/emission energy in the visible range has been achieved, making these 2D materials more attractive for photovoltaic applications.[14] Furthermore, 2D perovskite materials with tunable bandgaps show considerable potential in applications such as LEDs and lasers.[17,18]

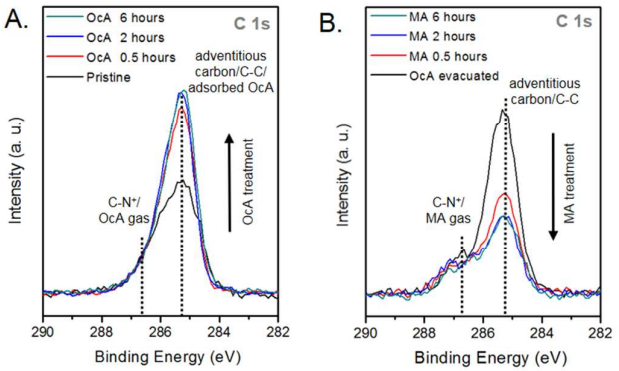

Figure 1. (A) C 1s photoelectron spectra of the $MAPbBr_3$ sample recorded at an OcA pressure of 0.7 mbar between 0-6 h. (B) C 1s photoelectron spectra of the OcA-treated $MAPbBr_3$ film recorded at an MA pressure of 0.7 mbar between 0-6 h.

Recently, the post-synthetic transformation of lead-halide perovskites has provided an opportunity to tune their optical and electronic properties flexibly and reversibly, further expanding the functionality of perovskite materials.[19,20] Due to interactions of different compounds with cations (e.g., MA^+), the optical and structural properties of pre-synthesized perovskite films were tuned.[21] Moreover, the post-synthetic method allows the morphology of the parent film to be preserved/improved in the product,[22,23] which affords perovskites with higher performance than those formed through traditional procedures.

Although the main focus of research has been to improve the materials' photovoltaic efficiency via reactions with different cations, there actually is very little known about the reaction mechanism, which limits the effective application of this post-synthetic method to form 3D/2D perovskite materials for high-efficiency solar cells. In this work, we report a systematic investigation of the chemical and structural transformation of $MAPbBr_3$ films exposed to a long-chain molecule (octylamine, OcA). Using ambient pressure X-ray photoelectron spectroscopy (AP-XPS) and X-ray diffraction (XRD) to monitor changes in the chemical

[a] Radiation Laboratory, University of Notre Dame, Notre Dame, IN 46556, USA.
[b] Department of Chemistry and Biochemistry, University of Notre Dame, Notre Dame, IN 46556, USA.
[c] Department of Physics, University of Notre Dame, Notre Dame, IN 46556, USA.
E-mail: Sylwia.Ptasinska.1@nd.edu
†Electronic Supplementary Information (ESI) available. See DOI: 10.1039/x0xx00000x

composition and crystal structure, respectively, we obtained insights into the mechanism of the cation exchange reaction. Moreover, we explored the possibility of reversing the reaction by exposing the OcA-treated films to methylamine (MA).

To study cation-exchange-induced transformations of perovskites, $MAPbBr_3$ films were prepared according to a procedure reported previously.[24] The forward (3D-to-2D) and reverse (2D-to-3D) reactions were investigated using AP-XPS, in which we examined the chemical evolution of the as-synthesized $MAPbBr_3$ perovskite films and the OcA-treated perovskite films under exposure to OcA or MA vapor. Figures 1, S1 and S2 show the C 1s, N 1s, Pb 4f, and Br 3d photoelectron spectra of $MAPbBr_3$ perovskites obtained at an OcA vapor pressure of 0.7 mbar exposed up to 6 h. As shown in Figures 1 and S2, the C 1s spectra for the pristine $MAPbBr_3$ film revealed two features at the binding energies (BEs) of 285.3 eV and 286.6 eV, attributed to adventitious carbon and carbon from the methylammonium cation (MA^+), respectively.[25] In the N 1s spectra (Figures S1 and S2), the spectral feature observed at 402.4 eV was characteristic of MA^+.[25] The appearance of a new peak in the N 1s spectra at 397.7 eV was due to the formation of surface-adsorbed OcA (Figure S2). As the duration of OcA treatment increased, the intensity of the C 1s peak at 285.3 eV increased significantly (Figure 1A). Because the hydrocarbon ($-CH_2-$) from both OcA^+ and surface adsorbed OcA have the same BE at 285.3 eV,[26] the enhanced intensities of the peak might result from the formation of OcA^+ and the surface-adsorbed OcA. Subsequently, the OcA vapor was evacuated after a 6-hour treatment. The elimination of absorbed OcA molecules was confirmed by the loss of a signal at 397.7 eV in the N 1s spectra (Figure S2B, spectrum f). After vapor evacuation, MA vapor was introduced at a pressure of 0.7 mbar for the reverse reaction. By exposing the OcA-treated perovskite sample to MA vapor, a gradual decrease was observed in the C 1s peak at 285.3 eV, which suggested the gradual loss of OcA^+. In contrast, no distinguishable changes were observed in the intensities of the peaks of the N 1s spectra before and after treatment with OcA and MA (Figure S1). The similar photoelectron intensity of N 1s corresponding to either MA^+ or OcA^+ implies that the nitrogen-containing species within the perovskite structure remained unchanged.

Figures 2A and S3 show the quantitative analysis of the contents of C and N relative to Pb, which was estimated from the fitted spectra of C 1s (285.3 eV), N 1s (402.5 eV), and Pb 4f. Upon exposure to OcA, the spectra of the perovskite film showed a rapid increase in the ratio of the C/Pb from approximately 3 to 22. After the OcA treatment, the evacuation of the vapor led to a gradual decrease in the C/Pb ratio, suggesting the removal of surface-adsorbed OcA. This ratio finally reached 7 after evacuation for 24 h. It is worth noting that this ratio (C/Pb=7) is still higher than the original ratio (C/Pb=3), suggesting the existence of OcA^+ in the sample. For the reverse reaction, due to exposure to MA, the C/Pb ratio decreased gradually to 3, indicating the loss of OcA^+. In contrast to the change in the C/Pb ratio, the constant ratio of N/Pb in Figure S3 implied that the nitrogen-containing species (OcA^+ and/or MA^+) within the perovskite structure remained unchanged. Therefore, the varying C/Pb ratios and constant N/Pb ratios indicated that the substitution occurs between equimolar amounts

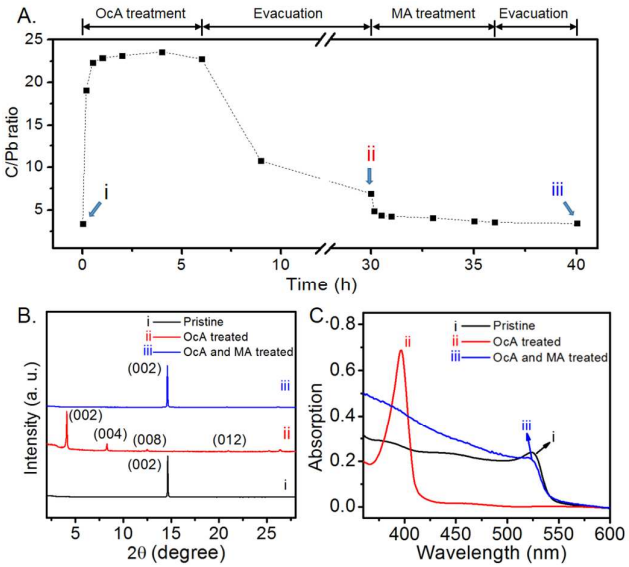

Figure 2. (A) Change of carbon (C) content relative to lead (Pb) in the $MAPbBr_3$ film as a function of time, as the sample was maintained continuously under the exposure of OcA for 6 h, in vacuum for 24 h, with exposure to MA for 6 h and then in vacuum for 3 h. The $MAPbBr_3$ films were treated under the same experimental conditions and used for XRD measurements, as the arrows indicate. (B and C) XRD pattern and UV-Visible spectra of (i) the pristine $MAPbBr_3$ film, (ii) the $MAPbBr_3$ film obtained after the exposure of OcA, and (iii) the $MAPbBr_3$ film obtained after consecutive exposure to OcA and MA.

of MA^+ and OcA^+ cations. The ratios of C/Pb and N/Pb suggested that the presence of OcA/MA vapor triggers a reversible substitution between OcA^+ and MA^+. The replacement of MA^+ with OcA^+ is achieved through a proton transfer mechanism,[25] in which a proton (H^+) is removed from MA^+ and accepted by a primary amine molecule (OcA) (Figure S4).

XRD measurements were performed to study the structural transformation of perovskite films. As shown in Figure 2B, the XRD pattern of the pristine film (spectrum i) matched well with the results of the 3D perovskite structure reported.[27] Under OcA treatment for 6 h, 3D perovskites were converted successfully into 2D perovskites (Figure 2B, spectrum ii). The small features appearing at 4°, 8.2°, 12.5°, 21.0°, and 26.5° were related to 2D $(OcA)_2PbBr_4$, as reported in the literature.[28] As shown in spectrum iii in Figure 2B, the XRD pattern of the 2D $(OcA)_2PbBr_4$ film treated with MA for 6 h showed a new diffraction peak at 14.5° that represented the 3D $MAPbBr_3$ crystalline structure. The reversible structural change was consistent with the chemical shift of the absorption edge for the perovskite samples observed. The transformation between 3D $MAPbBr_3$ and 2D $(OcA)_2PbBr_4$ produced a change in the absorption edges between 525 and 397 nm (Figure 2C).

To investigate further whether the cation exchange reaction changed the film morphology significantly, top-view and cross-section scanning electron microscopy (SEM) images of the perovskite samples were obtained. Figures 3A-C show the SEM top-view images of the as-synthesized $MAPbBr_3$ films and the films used

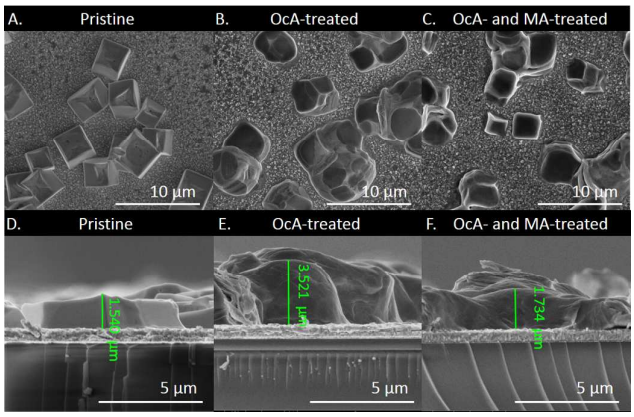

Figure 3. Top-view (A-C) and cross-section (D-F) SEM images of $MAPbBr_3$ films deposited on a FTO substrate: (A and D), the pristine film; (B and E), the film obtained after the exposure of OcA; and (C and F), the film obtained after consecutive exposure to OcA and MA.

in the forward and reverse reactions.

In the as-synthesized film, the $MAPbBr_3$ crystals had a cubic shape with lateral sizes of ~3-5 µm. Upon treatment with OcA vapor, the cubic particles merged with adjacent particles and formed larger $(OcA)_2PbBr_4$ particles, having a round shape. Interestingly, subsequent exposure to MA vapor did not cause complete recovery to the cube-shaped particles. The SEM cross-section images of the perovskite films are displayed in Figure 3D-F. As Figure 3D shows the as-synthesized $MAPbBr_3$ films had a thickness of ~1.5 µm. Furthermore, the SEM image in Figure 3E shows that the thickness of the film increased upon OcA treatment. This likely is due to the intercalation of the large molecules between layers. In contrast, when the reverse reaction occurred, the thickness of the perovskite films decreased (Figure 3F), suggesting the formation of a 3D perovskite structure.

Based on our experimental findings, it is evident that the reversible transformation of 3D-2D perovskite is triggered by an equimolar cation exchange. A plausible reaction mechanism for the reversible 3D-2D perovskites transformation through cation exchange was proposed (Figure 4 and reaction S1). In general, the structure of 3D hybrid perovskites is organized by the alternate stacking of organic/inorganic layers through attractive ionic interactions between the cationic and the $(PbX_6)^{4-}$ parts. With the addition of a long-chain ammonia cation (OcA^+), the cation exchange reaction occurs and the 2D layered perovskites are obtained, which is associated with the production of $PbBr_2$ and methylamine (Step 1 in Figure 4). However, no relative XRD features in the OcA-treated perovskite film could be attributed to those of $PbBr_2$, which indicates the formation of an amorphous feature in the Pb-Br solid.[29] In the reverse cation exchange reaction, the substitution of OcA^+ with small molecules (MA^+) occurred when MA was introduced (Step 2 in Figure 4).

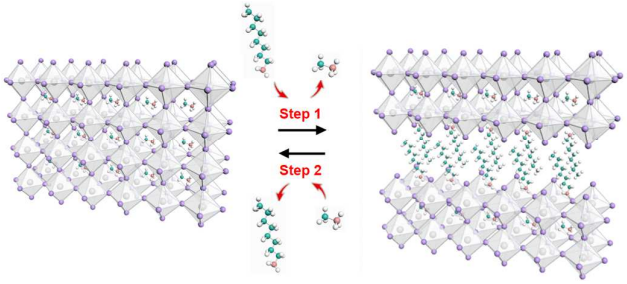

Figure 4. Schematic of the reversible transformation of 3D-2D perovskites. Steps 1 and 2 represent the forward and reverse reactions, respectively.

To summarize, reversible substitution reactions between MA^+ and OcA^+ were investigated using an *in situ* AP-XPS technique. The XPS analysis indicated that the presence of OcA triggered the transformation of $MAPbBr_3$ to $(OcA)_2PbBr_4$ via a cation exchange mechanism. We also demonstrated that the $(OcA)_2PbBr_4$ films can revert to $MAPbBr_3$ after exposure to MA. Furthermore, the XRD patterns suggested a reverse conversion between 3D and 2D perovskite structures. These results provide an essential understanding of cation-exchange-induced transformation of perovskites that might help exploit the unique properties of perovskites to develop more tunable and high-quality materials through post-synthetic modification.

This material is based upon work supported by the U.S. Department of Energy Office of Science, Office of Basic Energy Sciences under Award Number DE-FC02-04ER15533. This is contribution number NDRL 5206 from the Notre Dame Radiation Laboratory. The authors thank the cSEND Materials Characterization Facility for the use of the Bruker pXRD.

Conflicts of interest

There are no conflicts to declare

Notes and references

1 H. Zhou, Q. Chen, G. Li, S. Luo, T. -b. Song, H.-S. Duan, Z. Hong, J. You, Y. Liu and Y. Yang, Science, 2014, 345, 542–546.

2 J. S. Manser, J. A. Christians and P. V. Kamat, Chem. Rev., 2016, 116, 12956–13008.

3 M. L. Petrus, J. Schlipf, C. Li, T. P. Gujar, N. Giesbrecht, P. Müller-Buschbaum, M. Thelakkat, T. Bein, S. Hüttner and P. Docampo, Adv. Energy Mater., 2017, 7, 1700264.

4 M. I. Asghar, J. Zhang, H. Wang and P. D. Lund, Renew. Sustain. Energy Rev., 2017, 77, 131–146.

5 J. S. Manser, M. I. Saidaminov, J. A. Christians, O. M. Bakr and P. V Kamat, Acc. Chem. Res., 2016, 49, 330–338.

6 J. A. Christians, P. A. Miranda Herrera and P. V Kamat, J. Am. Chem. Soc., 2015, 137, 1530–1538.

7 W. Huang, J. S. Manser, P. V. Kamat and S. Ptasinska, Chem. Mater., 2016, 28, 303–311.

8 W. Huang, S. Sadhu and S. Ptasinska, Chem. Mater., 2017, 29, 8478–8485.

9 A. R. Milosavljević, W. Huang, S. Sadhu and S. Ptasinska, Angew. Chemie, 2016, 55, 10083–10087.

10 D. P. McMeekin, G. Sadoughi, W. Rehman, G. E. Eperon, M. Saliba, M. T. Hörantner, A. Haghighirad, N. Sakai, L. Korte, B. Rech, M. B. Johnston, L. M. Herz and H. J. Snaith, Science, 2016, 351, 151–155.

11 G. Niu, X. Guo and L. Wang, J. Mater. Chem. A, 2014, 0, 1–11.
12 I. C. Smith, E. T. Hoke, D. Solis-Ibarra, M. D. McGehee and H. I. Karunadasa, Angew. Chemie, 2014, 126, 11414–11417.
13 J. A. Sichert, Y. Tong, N. Mutz, M. Vollmer, S. Fischer, K. Z. Milowska, R. García Cortadella, B. Nickel, C. Cardenas-Daw, J. K. Stolarczyk, A. S. Urban and J. Feldmann, Nano Lett., 2015, 15, 6521–6527.
14 D. H. Cao, C. C. Stoumpos, O. K. Farha, J. T. Hupp and M. G. Kanatzidis, J. Am. Chem. Soc., 2015, 137, 7843–7850.
15 H. Tsai, W. Nie, J.-C. Blancon, C. C. Stoumpos, R. Asadpour, B. Harutyunyan, A. J. Neukirch, R. Verduzco, J. J. Crochet, S. Tretiak, L. Pedesseau, J. Even, M. A. Alam, G. Gupta, J. Lou, P. M. Ajayan, M. J. Bedzyk, M. G. Kanatzidis and A. D. Mohite, Nature, 2016, 536, 312–316.
16 T. Zhang, M. I. Dar, G. Li, F. Xu, N. Guo, M. Grätzel and Y. Zhao, Sci. Adv., 2017, 3, e1700841.
17 T. Zhang, L. Xie, L. Chen, N. Guo, G. Li, Z. Tian, B. Mao and Y. Zhao, Adv. Funct. Mater., 2017, 27, 1603568.
18 Y. Zhao and K. Zhu, Chem. Soc. Rev., 2016, 45, 655–689.
19 Q. A. Akkerman, V. D'Innocenzo, S. Accornero, A. Scarpellini, A. Petrozza, M. Prato and L. Manna, J. Am. Chem. Soc., 2015, 137, 10276–10281.
20 I. C. Smith, M. D. Smith, A. Jaffe, Y. Lin and H. I. Karunadasa, Chem. Mater., 2017, 29, 1868–1884.
21 G. Li, T. Zhang, N. Guo, F. Xu, X. Qian and Y. Zhao, Angew. Chemie Int. Ed., 2016, 55, 13460–13464.
22 Y. Zhou, M. Yang, S. Pang, K. Zhu and N. P. Padture, J. Am. Chem. Soc., 2016, 138, 5535–5538.
23 G. E. Eperon, C. E. Beck and H. J. Snaith, Mater. Horizons, 2016, 3, 63–71.
24 C.-G. Wu, C.-H. Chiang and S. H. Chang, Nanoscale, 2016, 8, 4077–4085.
25 W. Huang, J. S. Manser, S. Sadhu, P. V. Kamat and S. Ptasinska, J. Phys. Chem. Lett., 2016, 7, 5068–5073.
26 S. Alexander, L. Morrow, A. M. Lord, C. W. Dunnill, A. R. Barron and A. R. Barron, J. Mater. Chem. A, 2015, 3, 10052–10059.
27 L. Liu, S. Huang, L. Pan, L.-J. Shi, B. Zou, L. Deng and H. Zhong, Angew. Chemie Int. Ed., 2017, 56, 1780–1783.
28 S. Gonzalez-Carrero, G. M. Espallargas, R. E. Galian, J. Pérez-Prieto, Y. Oishi, C. H. A. Huan, T. C. Sum, C. Boissière, J. Pérez-Prieto, J.-S. Lauret and E. Deleporte, J. Mater. Chem. A, 2015, 3, 14039–14045.
29 H. Chen, X. Zheng, Q. Li, Y. Yang, S. Xiao, C. Hu, Y. Bai, T. Zhang, K. S. Wong and S. Yang, J. Mater. Chem. A, 2016, 4, 12897–12912.

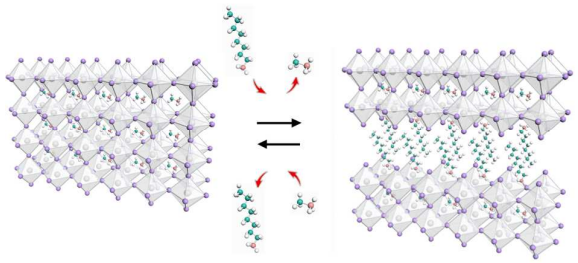

In situ XPS analysis shows that reversible transformation of 3D-2D perovskites can occur through post-synthetic introduction of new cations.